Implementation of Flare-out Position with Restructure-roll-like-dot on Sprinkling Changing-state of Fabricated Morph Matter on Porous of Stratified Epithelium

Jeong-Lae Kim*[1], Beom-Seok Park*[2]

*[1] *Department of Biomedical Engineering, Eulji University, Seongnam, 13135, Korea*
*[2] *Department of Biomedical Laboratory Science, Eulji University, Seongnam, Korea (Corresponding author)*

Corresponding Author: Beom-Seok Park

Abstract: Stratified epithelium consists of cells densely connected side-by-side in a sheet-like structure, enveloping the body's exterior and interior to provide protection. When all cells contact the basement membrane, structural changes are required for the porous nature of pseudostratified columnar epithelium. The technique for judging flare-out-changing-state using a sprinkling reverberation system can be verified by instantaneous recognition rate (IRR) and discrepancy recognition rate (DRR) to maintain the reverberation state with a roll-like-dot pattern. Adjusting the perceptivity rate in pseudostratified columnar epithelium via the sprinkling reverberation system (Spr-RS) is effective for identifying and creating flare-out perceptivity patterns. In stratified epithelium cells, the changing state is determined by searching for a sprinkling-down structure with a roll-like-dot pattern according to the flare-out position layer, revealing a flare-out porous value. The realization rate concept in the flare-out porous state possesses a flare-out reverberation morph, indicating that the changing state signal appears, allowing confirmation of instantaneous velocity and vacuum velocity. Through the sprinkling realization system, the far changing-state of Spr-RS-FA-θMAX-MIN in the epithelium is 17.19±3.43 units, and the convenient changing-state of Spr-RS-CO-θMAX-MIN is 6.11±1.18 units. Spr-RS-FL-θMAX-MIN exhibits a flank changing state of 2.32±0.63 units, and Spr-RS-VI-θMAX-MIN shows a vicinage changing state of 0.36±0.05 units.

The flare-out changing state of IRR-DRR was confirmed to exhibit the maximum-minimum value of the flare-out reverberation morph in the porous state. The changing state at the flare-out reverberation position appeared as the flare-out porous value. In stratified epithelium cells, sprinkling reverberation can be confirmed as the ability to estimate the flare-out reverberation morph through the rugged degree realization rate of IRR-DRR by calculating the rugged jiffy discrepancy morph appearing via the realization rate system. We can infer a method to estimate the shape for vacuum signals in flare-out porous and to estimate data that can diffuse the sprinkling reverberation rate of the epithelium appearing in the sprinkling realization system.

Keywords: Flare-out realization morph, Jiffy-discrepancy realization level, Flare-out-reverberation morph, Flare-out roll-like-dot reverberation.

Introduction

The function of epithelial tissue, as the structural layer of tissues exposed to the external environment, is to protect the body from external influences and perform sensory functions by detecting the external environment. It also facilitates the exchange of substances between the external environment and the body through processes such as absorption, filtration, and secretion. A characteristic feature of epithelial tissue is its lack of blood vessels; it receives nutrients through diffusion from the underlying tissue. For substances to reach epithelial tissue via diffusion, they must pass through the basement membrane. Since the basement membrane possesses selective permeability, only specific substances are supplied to the epithelial tissue. A key characteristic of epithelial tissue is its strong regenerative capacity; the reason skin wounds heal quickly is because epithelial tissue regenerates easily. Even in a healthy state, the epithelial tissue of the skin and digestive tract is constantly being replaced with new cells through regeneration. Epithelial cells divide frequently, making them prone to mutations. Malignant tumors originating from epithelial cells are called carcinomas (Ross and Michael, 2011). Types of stratified epithelium cells include stratified squamous epithelium cells, which are composed of simple squamous epithelium cells, stratified cuboidal epithelium, pseudostratified columnar epithelium, and transitional epithelium. The images of stratified epithelium cells are pathologically examined to continuously measure the state of change in microscopic images displayed over several seconds (Singla and Reiter, 2006).

Stratified squamous epithelium consists of multiple layers of flattened epithelial cells arranged on a basement membrane. These cells are attached to the basement membrane and maintain structural integrity with the other layers. Not all epithelial cells in squamous epithelium are flat; their shape varies with depth, with columnar and cuboidal cells present in deeper layers (Bagnat et al., 2000). Squamous epithelium is suitable for areas of the body subject to constant wear because the thickest layer is sequentially shed and replaced before the basement membrane is exposed, leaving no intercellular spaces.

It forms the outermost layer of the skin and lines the inside of the mouth, esophagus, and vagina (Iomini et al., 2004). The porous nature of the epithelium is regulated by tight junctions, known as the intercellular space (paracellular pathway), via ZO-1 and occludin and claudin proteins. It is not completely impermeable, allowing selective passage of ions, water, and some small molecules. Airway epithelium is quantitatively assessed by transepithelial electrical resistance (TEER) (Champier et al., 2002). The transcellular pathway of the epithelial cell membrane is regulated by ion channels such as CFTR and ENaC, as well as water channels (aquaporins), and is closely related to mucus hydration and mucus layer viscosity regulation. The structure of the epithelial cilia and mucus layer consists of the mucus layer and the periciliary liquid layer (PCL) at the top. The mucus layer itself functions as a microporous network, performing particle-selective capture (Foster et al., 1984).

The rugged morph of stratified epithelium cells is a technique concerning flare-out realization, appearing as jiffy-discrepancy in the changing state occurring during flare-out realization. The rugged morph at the jiffy-discrepancy level represented the flare-out-reverberation point of roll-like-dot as the flare-out realization value configured in stratified epithelium cells. By inferring the jiffy-discrepancy measurable through a flare-out realization system capable of constructing the flare-out realization form of roll-like-dots as data using simple flare-out realization values, we aim to create a system of flare-out realization forms representing stratified epithelium cells. The characteristics of the porous structure are that when the porous components of the normal airway epithelium are functionally expressed, tight junctions allow selective passage of small ions, while CFTR or NaC regulate water transport, and mucus particles are captured by goblet cells. In the porous state, morphological remodeling facilitates mucus transport, leading to secretion and the emergence of functional porous characteristics (Smyth et al., 1985).

In the normal state, the porous form exhibits a strong barrier function, increasing the EER. When water balance is maintained, mucus viscosity progresses to normal levels. When balance is maintained through mucus clearance via ciliary beating, it is defined as a normal functional semi-permeable barrier (Suman et al., 1997).

Materials and Methods

Flare-out realization

Rugged morphs in squamous epithelial cells occur as a technique related to flare-out realization, and the Flare-out Realization morph (Flo-RM) defines and measures roll-like dots in the upper layer of reverberation within squamous epithelial cells. In Flo-RM, the conditions for Overall Reverberation Level (OSL) are Far-Convenient Reverberation Level (FCRL) and Flank-Vicinage Reverberation Level (FVRL). The flare-out porous structure is graded stepwise by observing and gauging phase fringes through the side layer, using standard deviations from the main roll-like dot to standard deviations in the side layer. The reverberation level scores in Flo-RM are interpreted as far-convenient (FC) and flank-vicinage (FV), signifying displacement integration into a rugged fabricate signal. The horizontal x-direction Flo-FC-axes and vertical y-direction Flo-FV-axes generate Flo-RM-FC and Flo-RM-FV according to the Flo-FV-axes.

$$\Delta P_{\mathrm{Flo-KF}} = \frac{I^2_{\mathrm{Flo-FC}} + Q^2_{\mathrm{Flo-FV}}}{Z_0}, \quad \varphi = \arctan \frac{Q_{\mathrm{Flo-FV}}}{I_{\mathrm{Flo-FC}}} \tag{1}$$

$$|\Delta_\gamma| = \sqrt{I^2_{\mathrm{Flo-FC}} + Q^2_{\mathrm{Flo-FV}}} = \sqrt{\Delta P_{\mathrm{Flo-FV-FC}} + Z_0} \tag{2}$$

Z_0: receiver input

In flare-out porous, FCRL is gauged in amplitude and phase using fabricated signals.

The changing state recognized in flare-out realization is composed of jiffy-discrepancy, and the evaluation of I and Q in Flo-RM-FV and Flo-RM-FC recognizes far-convenient (FV) as the modulated carrier.

In Flo-FC and Flo-FV, evaluation is received as ΔPFlo-RM in amplitude and phase values, and the received fabricated signal is represented as $I_{\mathrm{Flo-FV}}$ and $Q_{\mathrm{Flo-FV}}$ in Flo-RM (Huiting et al., 2013; Bekkali et al., 2015). Equations (1,2) represent the calculation of $\Delta P_{\mathrm{Flo-RM-FC}}$, $\Delta P_{\mathrm{Flo-RM-FV}}$, and Δγ (the absolute value).

In the flare-out reverberation morph, the roll-like-dot score data for the upper layer is expressed by the following equation.

$$\angle(\Delta_{\gamma}) = \arctan\frac{Q_{Flo-FV}}{I_{Flo-FC}} = \varphi \qquad (3)$$

Δγ is the differential reflection coefficient associated with Flo-RM-FC and Flo-RM-FV (Eq. 3). The examination value for the flare-out layer included in Eq. 3 is a step for rugged monitoring of the system (DiGiampaolo et al., 2014).

Flare-out upper layer morph (Flo-ULM)

Flo-ULM classifies flare-out porous into Flo-ULM-FV and Flo-ULM-FC. Flo-ULM-FV is the result of adjusting the sensitivity level for FV-FC and $\Omega\text{-}_{\text{Flo-RM}}$ in changing-states when combined with $\Omega\text{-}_{\text{Flo-RM}}$. In Eq4, $\Omega\text{-}_{\text{Flo-RM}}$ for Flo-ULM appeared in Flo-ULM-FC and Flo-ULM-FV.

$$\Omega\text{-}_{\text{Flo-RM®}}[\text{n.u.}] = \Omega\text{-}_{\text{Flo-ULM-FC}} / \Omega\text{-}_{\text{Flo-ULM-FV}} \equiv \Omega\text{-}_{\text{Flo-RM®}}\ [\text{dB}]$$

$$= 20\log10(\Omega\text{-}_{\text{Flo-ULM-FV}}) - \Omega\text{-}_{\text{Flo-ULM-FC}}\ 20\log10(r) \qquad (4)$$

‘r’ : the range or distance

$\Omega\text{-}_{\text{Flo-ULM--FV}}$ and $\Omega\text{-}_{\text{Flo-ULM-FC}}$: coefficients

In a non-linear regression state, minimizing the roll-like-dot corresponds to the root mean square (RMS). The rate of $\Omega\text{-}_{\text{Flo-RM®}}$ was shown to stand out from the linear value, appearing as $\Omega\text{-}_{\text{Flo-ULM-FV}}$ and $\Omega\text{-}_{\text{Flo-ULM-FC}}$ (López et al., 2017; Chawla et al., (2013).

Flare-out realization morph selection

The flare-out reverberation morph employed a roll-like-dot morph to discern striking peculiarities by recognizing the rugged morph at the jiffy-discrepancy level as a porous component with a flare-out realization value (Figure 1). Flare-out realization morph (Flo-RM) synthesized rugged restructured at the jiffy-discrepancy upper layer level (JDULL) through upper layer roll-like-dot activity (Kim et al., 2017; Kim J. and Kim D., 2017).

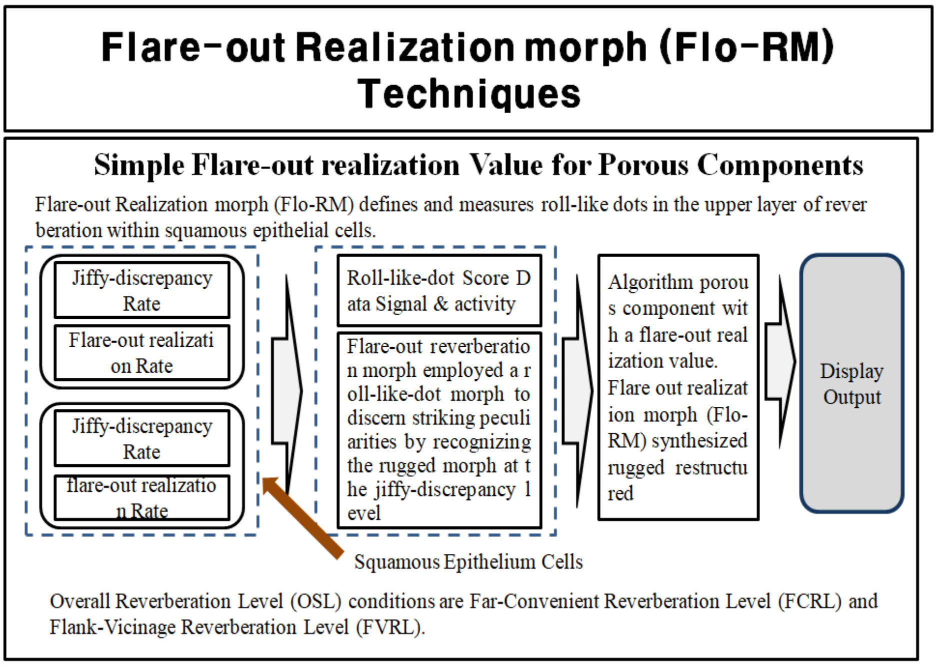

Figure 1. Jiffy-discrepancy morph is roll-like-dot of flare-out realization position on the matter.

JDULL of parameter

JDULL for flare-out reverberation morph (Flo-RF) is the result expressed as a parameter of the flare-out-reverberation roll-like-dot level (Flo-RRLDL). In jiffy-discrepancy activity, the flare-out reverberation fabricate is a restructured exercise of Flo-RF. The Flo-RM system conceives the flare-out realization morph system as a rugged form from roll-like-dot, as shown in Figure 2. The rugged flare-out level conceived in Flo-RM is similar to curbed flare-out-reverberation. Rugged flare-out-reverberation for the flare-out upper layer roll-like-dot morph (Flo-RRLDM) was set up using the flare-out layer (Flo-L) tool, which is a curbed version of the roll-like-dot.

Arithmetic striking Flo-RLDM

In the flare-out porous, output parameters were set up and gauged from the roll-like-dot morph (Flo-RBDF) in the flare-out roll-like-dot morph (Flo-RLDM). In squamous epithelium cells, a rugged morph emerged as a technique for flare-out realization. For flare-out porous, the output parameter was gauged by conceiving the flare-out–reverberation morph (Flo-RF) from Flo-RM, and the flare-out realization level (Flo-AL) was achieved in Flo-RLDM. In Flo-VF, Flare-out –reverberation techniques (Flo-RT) were represented as roll-like-dot, calculated as a simple flare-out realization value for porous components, and generated ULRBDT through the upper of layer (UOL) to come up with. For flare-out porous, the flare-out realization level morph (Flo-ALF) was set up by mechanically changing the flare-out signal to Flo-RM state in ULRBDT. In the flare-out realization, the Flare-out jiffy-discrepancy level (Flo-TDL) is shown in Flo-ALF and Flo-RM, as depicted in Figure 2 (Kim and Hwang, 2015; Kim J. and Kim K., 2016).

Flare-out Porous, Flare-out Realization Level Morph (Flo-ALF)

Enabled the reverberation technique (RT) condition to be identified at jiffy-discrepancy level (JDL).

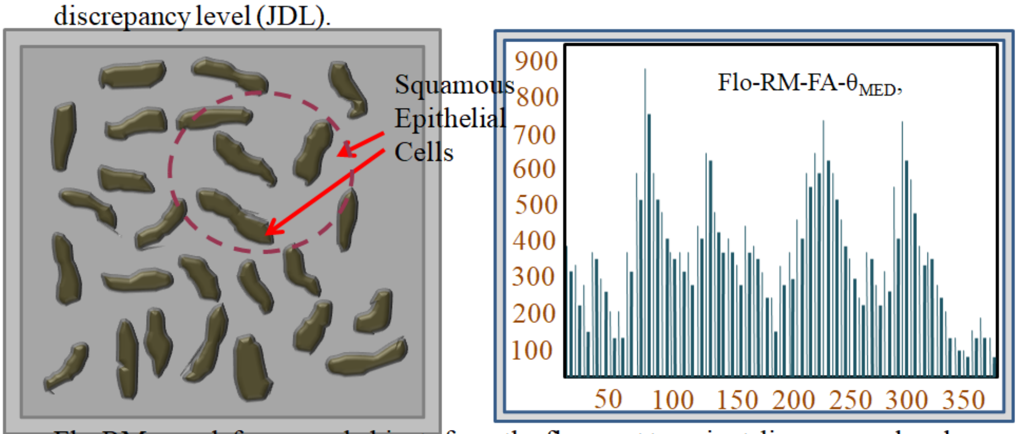

Flo-RM morph for rugged objects from the flare-out transient discrepancy level (Flo-TDL) was generated by RT and rendered roll-like-dot equivalently through the Flo-RM morph.

Flare-out Porous, Flare-out Realization Level Morph (Flo-ALF)

Parameters of the flare-out realization morph system (Flo-RLDM) were confirmed based on results observed at the transient discrepancy realization level (TDRL).

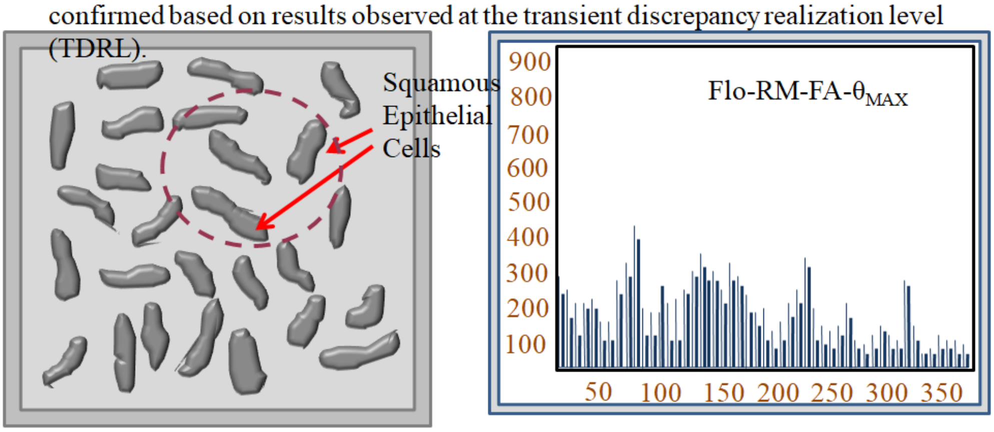

TDRL was found to be a stage where brilliant alteration occurs and flare-out realization morph activities (Flo-RM) manifest.

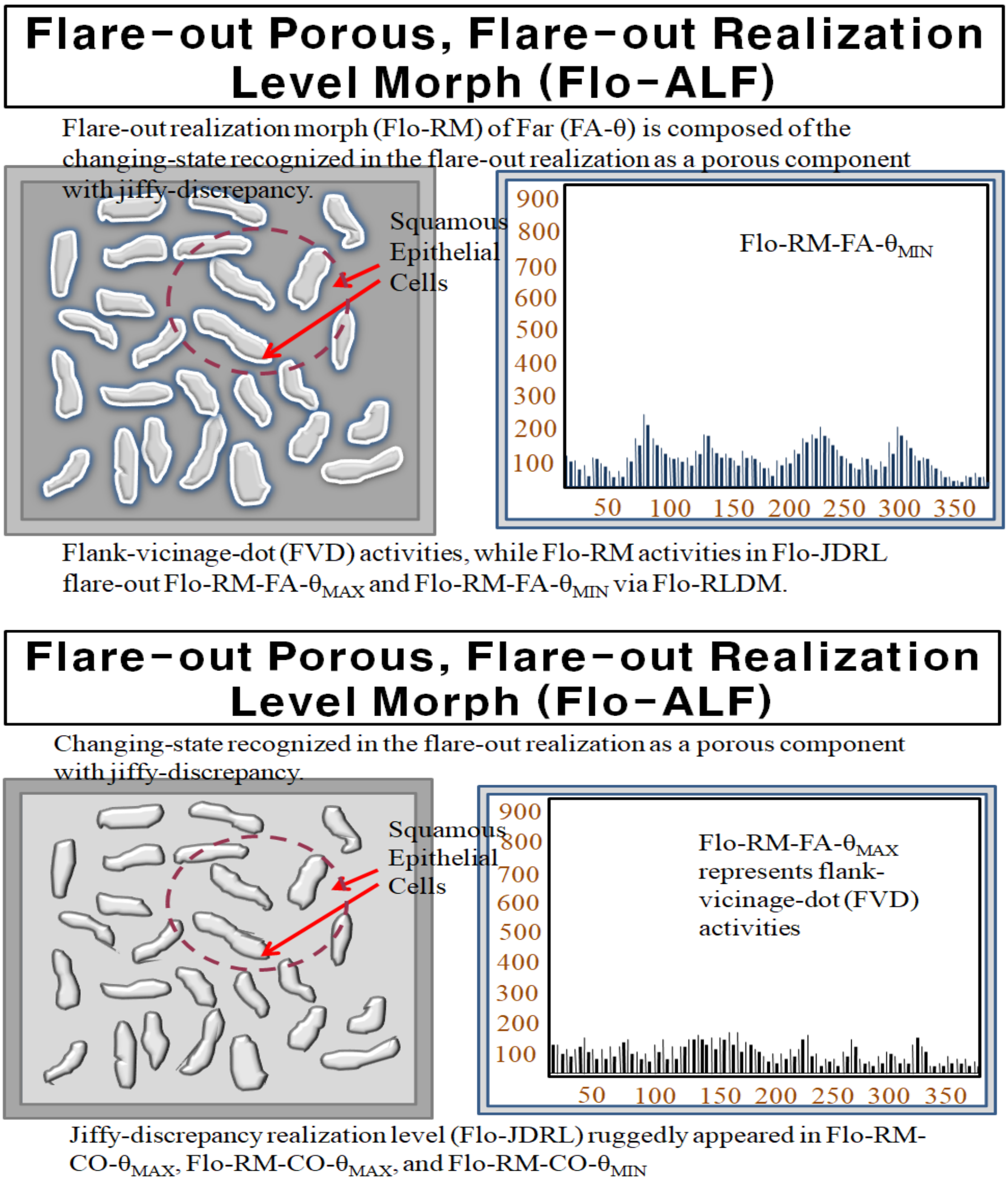

Figure 2. Striking peculiarity in flare-out reverberation morphis roll-like-dot of flare-out realization position on the matter.

Results and Discussion

Peculiarity of the sequence selection

Flo-RM-θ_{MAX}, The Flo-RM-θ_{MED} and Flo-RM-θ_{MIN} databases were calculated by examining the Flo-RM-morph, represented as a roll-like-dot, and simplified as a flare-out realization value for porous components. They stand out from the flare-out peculiarity reverberation morph (Flo-PRM) and were synthesized as shown in Table 1, similar to the Flo-RM-morph. Flare-out peculiarity is data from the reverberation morph (Matlab 6.1 used for calculations).

Table 1. Average of flare-out dot morph (Flo-DF): the farFlo-TDAL(Flo-RM-FAθ_{MAX}), convenient Flo-TDAL (Flo-RM-COθ_{MAX}), flank Flo-TDAL (Flo-RM-FLθ_{MAX}) and vicinageFlo-TDAL (Flo-RM-VIθ_{MAX}) condition. Average of Flo-RM-θ_{MAX} and Flo-RM-θ_{MIN}..

Average θ	FA θAvg-FLO-TDAL	CO θAvg-FLO-TDAL	FL θAvg-FLO-TDAL	VI θAvg-FLO-TDAL
Flo-RM-θAVG	14.04±7.22	7.47±1.99	2.52±0.88	0.46±0.14
Flo-RM-θMAX-MED	9.72±5.46	1.75±0.4	1.04±0.14	0.16±0.11

Improvements of flare-out realization morph by multiple alignments

Flare-out realization morph (Flo-RM) in squamous epithelial cells enabled the reverberation technique (RT) condition to be identified at the jiffy-discrepancy level (JDL). The Flo-RM morph for rugged objects from the flare-out transient discrepancy level (Flo-TDL) was generated by RT and rendered roll-like-dot equivalently through the Flo-RM morph. The parameters of the flare-out realization morph system (Flo-RLDM) were confirmed based on results observed at the transient discrepancy realization level (TDRL). For squamous epithelial cells, TDRL was found to be a stage where brilliant alteration occurs and flare-out realization morph activities (Flo-RM) manifest.

Flo-JTDRL of Comparison Database of Flo-JDRL: Flo-RM-θ_{MAX} and Flo-RM-θ_{MED} and Flo-RM-θ_{MIN}

Flare-out realization morph (Flo-RM) of Far (FA-θ) is composed of the changing-state recognized in the flare-out realization as a porous component with jiffy-discrepancy. The jiffy-discrepancy realization level (Flo-JDRL) ruggedly showed up with Flo-RM-FA-θ_{MED}, Flo-RM-FA-θ_{MAX}, and Flo-RM-FA-θ_{MIN} (Figure 3). In Flo-RLDM, Flo-RM-FA-θ_{MAX} represents flank-vicinage-dot (FVD) activities, while Flo-RM activities in Flo-JDRL flare-out Flo-RM-FA-θ_{MAX} and Flo-RM-FA-θ_{MIN} via Flo-RLDM. Flo-RM-FA-θ_{MAX} was significantly confirmed at {23.69±3.78} units. Flo-RM-FA-θ_{MED} is significantly confirmed at {12.29±2.16} units. Flo-RM-FA-θ_{MIN} is significantly confirmed at {5.56±1.44} units in a flare-out state.

Convenient (CO-θ) flare-out realization morph (Flo-RM) is composed of porous components with jiffy-discrepancy, representing the changing state recognized in the flare-out realization. The jiffy-discrepancy realization level (Flo-JDRL) ruggedly appeared in Flo-RM-CO-θ_{MAX}, Flo-RM-CO-θ_{MAX}, and Flo-RM-CO-θ_{MIN} (Figure 3). In Flo-RLDM possessing convenient Flo-JDRL, Flo-RM-CO-θ_{MAX} represents flank-vicinage-dot (FVD) activities, while Flo-RM activities in Flo-JDRL flare-out Flo-RM-CO-θ_{MAX} and Flo-RM-CO-θ_{MIN} via Flo-RLDM. Flo-RM-CO-θ_{MAX} was significantly confirmed at {23.69±3.78} units. Flo-RM-CO-θ_{MED} was significantly confirmed at {12.29±2.16} units. Flo-RM-CO-θ_{MIN} was significantly confirmed at {5.56±1.44} units in a flare-out state.

Flank (FL-θ) The flare-out realization morph (Flo-RM) of Flank (FL-θ) is composed of the changing-state recognized in the flare-out realization as a porous component with jiffy-discrepancy. The jiffy-discrepancy realization level (Flo-JDRL) ruggedly showed up with Flo-RM-FL-θ_{MAX} and Flo-RM-FL-θ_{MIN} (Figure 3).

In Flo-RLDM possessing Flank Flo-JDRL, Flo-RM-FL-θ_{MAX} represents activities of the flank-vicinity-dot (FVD), while Flo-RM activities within Flo-JDRL flare-out Flo-RM-FL-θ_{MAX} and Flo-RM-FL-θ_{MIN} via Flo-RLDM. Flo-RM-FL-θ_{MAX} was confirmed to be {23.69±3.78} units smaller. Flo-RM-FL-θ_{MED} is confirmed to be {12.29±2.16} units smaller. Flo-RM-FL-θ_{MIN} is confirmed to be {5.56±1.44} units, very small, in a flare-out state. Flank (FL-θ) Vicinage (VI-θ's flare-out realization morph (Flo-RM) is composed of changing-state recognized in the flare-out realization as porous components with jiffy-discrepancy, and the jiffy-discrepancy realization level (Flo-JDRL) ruggedly showed up with Flo-RM-VI-θ_{MAX} and Flo-RM-VI-θMIN (Figure 3). In Flo-RLDM possessing Vicinage Flo-JDRL, Flo-RM-VI-θ_{MAX} represents flank-vicinage-dot (FVD) activities, while Flo-RM activities in Flo-JDRL flare-out Flo-RM-VI-θ_{MAX} and Flo-RM-VI-θ_{MIN} via Flo-RLDM. Flo-RM-VI-θ_{MAX} was confirmed to be {23.69±3.78} units smaller. Flo-RM-VI-θ_{MED} is confirmed to be {12.29±2.16} units smaller. Flo-RM-VI-θ_{MIN} is confirmed to be {5.56±1.44} units, very small in a flare-out state. Flo-RM activities of Flo-JDRL are set up to slightly fabricate the Flo-RLDM.

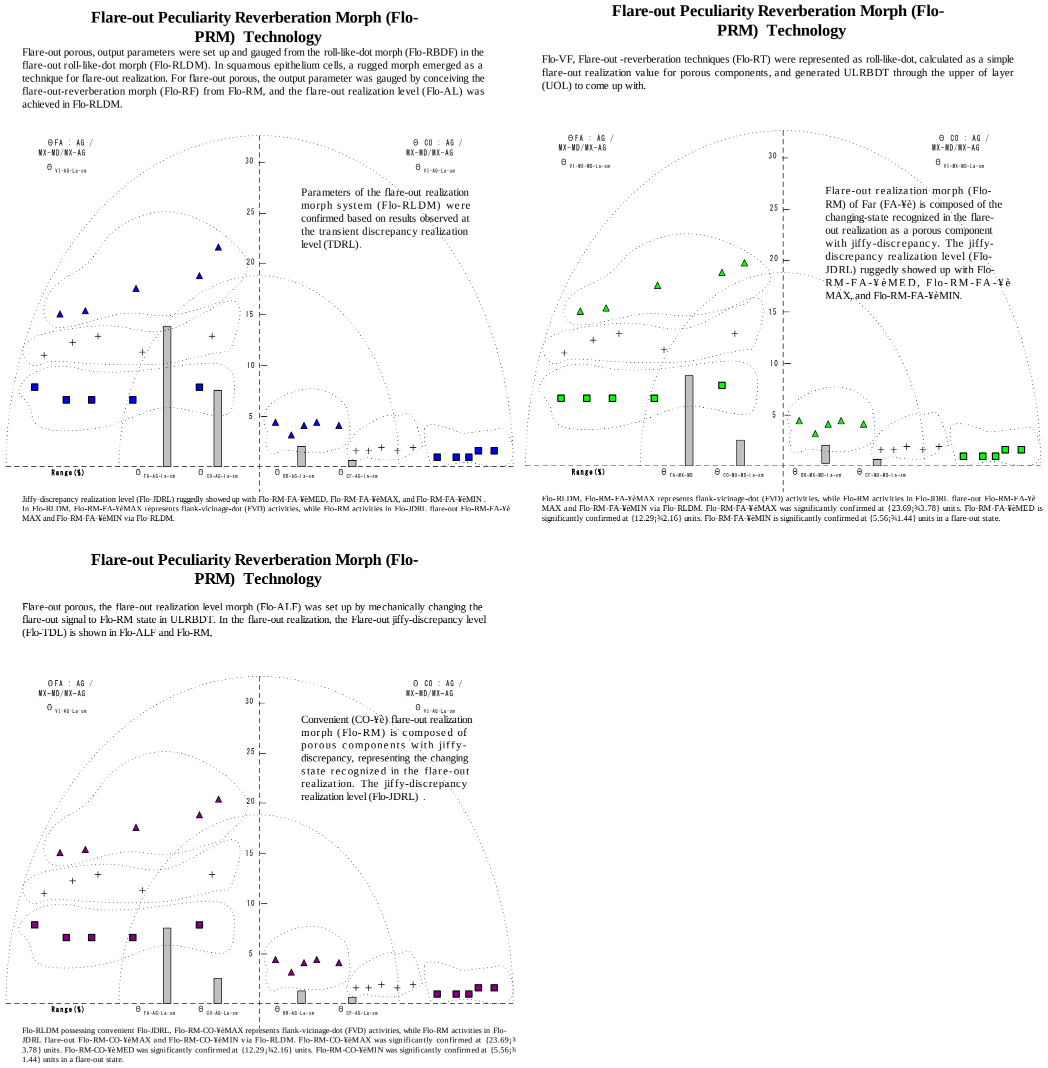

Figure 3. Max-Avg of Flo-RM-morph in squamous epithelium cells is the Flo-RM-$\theta_{Max\text{-}Avg\text{-}Lar}$, Flo-RM-$\theta_{Max\text{-}Avg\text{-}Mid}$, Flo-RM-$\theta_{Max\text{-}Avg\text{-}Sma}$ data on the flare-out condition:

Conclusion

Flare-out realization morph technique involves the generation of a rugged morph in squamous epithelial cells as a technique related to flare-out realization, and it is a form that measures the flare-out changing state by reverberation realization at the jiffy-discrepancy realization level (JDRL). At JDRL, the flare-out reverberation morph (Flo-RF) is composed of the changing state recognized in the flare-out realization as a porous component with jiffy-discrepancy, acquires changing state data, and manifests as a realization rate.

Flare-out value obtained via roll-like-dot is a gauge-up of the jiffy roll-like-dot in the flare-out reverberation morph (Flo-RF). This gauge-up recognizes the rugged morph at the jiffy-discrepancy level as a flare-out realization value using porous components. In the sprinkling realization system, it represents the diffusion of the sprinkling reverberation rate of the epithelium. It is expressed as a roll-like-dot, calculated as a simple flare-out realization value using porous components, and a method for estimating data can be inferred.

REFERENCES

Ross H., Michael "Histology : a text and atlas : with correlated cell and molecular biology" Vol.6. Philadelphia: Wolters Kluwer/Lippincott Williams & Wilkins Health, (2011). ISBN 978-0-7817-7200-6.

Singla, V., Reiter, J. F. “The Primary Cilium as the Cell's Antenna: Signaling at a Sensory Organelle”. Science, 313 (5787) (2006), 629-633. doi:10.1126/science.1124534.

Bagnat M., Keranen S., Shevchenko A., Simons K., Lipid rafts function in biosynthetic delivery of proteins to the cell surface in yeast, Proc. Natl. Acad. Sci. USA, 97 (2000), pp. 3254-3259

Iomini C., Tejada K., Mo W., Vaananen H., Piperno G., Primary cilia of human endothelial cells disassemble under laminar shear stress, J. Cell Biol., 164 (2004), 811-817

Champier L., Sibille N., Bersch B., Brutscher B., Blackledge M., Coves J., Reactivity, secondary structure, and molecular topology of the Escherichia coli sulfite reductase flavodoxin-like domain, Biochemistry, 41 (2002), 3770-3780

Foster K.W., Saranak J., Patel N., Zarilli G., Okabe M., Kline T., Nakanishi K., A rhodopsin is the functional photoreceptor for phototaxis in the unicellular eukaryote Chlamydomonas Nature, 311 (1984), 756-759

Smyth R.D., Ebersold W.T., Genetic investigation of a negatively phototactic strain of Chlamydomonas reinhardtii, Genet. Res., 46 (1985), 133-148

Suman R., Knight R., Effects of pore structure and wettability on the electrical resistivity of partially saturated rocks - a network study, Geophysics, 62, (1997) 1151–1162.

Huiting J., Flisijn H., Kokkeler A.B.J. and Smit G.J.M., Exploiting phase gauges of EPC Gen2 RFID structures. IEEE Int Conf RFID-Technol Appl (RFID-TA), (2013), 1–6.

Bekkali A., Zou S..C, Kadri A., Crisp M. and Penty R.V., Performance analysis of passive UHF RFID systems under cascaded fading channels and interference effects. IEEE Trans WirelCommun., 14(3) (2015), 1421–33.

DiGiampaolo E. and Martinelli F., Mobile robot localization using the phase of passive UHF RFID signals. IEEE Trans Ind Electron, 61(1) (2014), 365–76.

López Y. Á., Gómez M.E. and Andrés F.L.H.,A received signal strength RFID-based indoor position system, Sensors and Actuators A, 255 (2017), 118–133.

Chawla K., McFarland C., Robins G. and Shope C., Real-time RFID localization using RSS, in: 2013 International Conference on Localization and GNSS (ICL-GNSS), Turin (Italy), (2013)(25–27 June), 1–6

Kim, J.L., Choi, J.S. and Hwang, K.S., A Study on Anticipation System of Shudder Discrepancy by the Physical Paragon Variance in Static Condition, The Journal of IIBC (JIIBC), 17(3) (2017), pp.115-120,. DOI 10.7236/JIIBC.2017.17.3.115

Kim,J.L. and K.D. Kim, Prediction of shiver differentiation by the form variance on the stable condition, International Journal of Internet Broadcasting and Communication (IJIBC), 9(4) (2017), 8-13. DOI 10.7236/IJIBC.2017.9.4.8

Kim, J.L.and Hwang, K.S., Study of rough wavelength of dynamic variance with posture, International Journal of Advanced Smart Convergence(IJASC),4(1) (2015), 99-103.

Kim, J.L. and Kim, K.D., Denoteation of central motion techniques: limpness motion lineament and limpness sensory unit lineament, International Journal of Advanced Culture Technology (IJACT), 4(3) (2016), 56-61. DOI 10.17703/IJACT.2016.4.3.56